

Bio-inspired hierarchical designs for stiff, strong interfaces between materials of differing stiffness

Daniel Rayneau-Kirkhope^{1,2,*}, Yong Mao³, Cyril Rauch⁴

¹ *Aalto Science Institute, School of Science, Aalto University, 02150 Espoo, FINLAND*

² *Department of Applied Physics, Aalto University, 02150 Espoo, FINLAND*

³ *School of Physics and Astronomy, University of Nottingham, NG7 2RD, UK*

⁴ *School of Veterinary Medicine and Science, University of Nottingham, Sutton Bonington, LE12 5RD, UK*

(Dated: July 20, 2018)

Throughout biology, geometric hierarchy is a recurrent theme in structures where strength is achieved with efficient material usage. Acting over vast timescales, evolution has brought about beautiful solutions to problems of mechanics that are only now being understood and incorporated into engineering designs. One particular example of structural hierarchy is found in the junction between stiff keratinised material and the soft biological matter within the hooves of ungulates. Using this biological interface as a design motif, we investigate the role of hierarchy in the creation of a stiff, robust interface between two materials. We show that through hierarchical design, we can manipulate the scaling laws relating constituent material stiffness and overall interface stiffness under loading. Furthermore, we demonstrate that through use of a hierarchical geometry, we can reduce the maximum stress the materials experience for a given loading, and tailor the ratio of maximum stresses in the constituent materials. We demonstrate that when joining two materials of different stiffness hierarchical geometries are linked with beneficial mechanical properties and enhanced tailorability of mechanical response.

I. INTRODUCTION

Naturally occurring hierarchical interfaces for adhesion between two surfaces have been well documented, examples of such designs are to be found on the feet of geckos, spiders and insects [1–3]. Although other contributions have been identified [4], it is understood that the primary interaction allowing geckos to walk up walls is the van der Waals interaction [5, 6]. The hierarchical geometry of the gecko’s foot is key in making this adhesion possible utilising this very weak interaction [7]. This structure has inspired a research area with the goal of creating dry adhesive mechanisms [8–11]. Other fractal-like geometries are found in nature suited to various functionalities including spider capture silk for strength and elasticity [12], biological composites for stiffness and fracture toughness [13, 14] and trabecular bone for stiffness and minimal weight [15]. Recently, novel manufacturing methods have allowed the principles of geometric hierarchy to be utilised in engineering design [16–19].

Structures that derive their mechanical properties predominantly from their geometry rather than their material composition are often referred to as mechanical metamaterials [20]. Utilising geometry to control the mechanics of a system can lead to novel, beneficial properties, including auxetic response [21, 22], energy trapping [23], mechanical cloaks [24], and high strength to weight ratios [25]. Here we look to control the mechanical response of a system made up of three materials through controlling the geometry of the structure, in particular, we investigate the effect of adding geometric hierarchy.

It is widely observed that naturally occurring interfaces with non-trivial geometry exhibit remarkable mechanical properties [26–28]. Suture joints are a prime example of such geometric specialisation for mechanical purposes, such joints are typically observed joining two regions of a given material via an interfacial region comprised of a second material with a lower stiffness [28, 29]. Examples of such joints are to be found in bone [2] (including the cranium [30]), turtle shell [29] and ammonites [14, 31]. In all of these cases, mechanical function (including stiffness, strength, fracture/penetration resistance) is hypothesised to be a driving factor in the design of the interface; other functions for which such designs are specialised include growth, respiration and buoyancy control [14, 30, 31]. While a range of geometries joining two domains of a given material utilising a second joining material (glue) have been extensively studied [2, 7, 14, 26–31], the problem of joining two materials of differing stiffness has received little attention. This problem is of particular interest where dissimilar materials enables designs to achieve a high structural efficiency in situations where stiffness, strength or damage tolerance are all of relevance [32].

In this paper, we focus on a novel application of hierarchical design – creating a permanent adhesive connection between two materials of differing stiffness. The geometry of both sides of the interface is designed to permit maximal interface stiffness and strength. The geometry we investigate is biologically inspired, we observe this particular geometry marking the transition from a stiff material to a softer material in equine and bovine hooves (figure 1), here we investigate whether this form could be a specialization linked with mechanical function. One of the adaptations of the equine hoof observed at this junction is its a hierarchical structure of laminae

*daniel.rayneau-kirkhope@aalto.fi

or lamellae [33, 34]. Approximately 600 primary epidermal lamellae, each bearing 100–150 non-keratinised secondary epidermal lamellae, increase the area for the adhesion between and dermis and epidermis to more than 2 m² [35]. Between the dermis and epidermis is a set of biological molecules allowing tissue to remain bounded together [36, 37]. The geometry of this interface is assumed to be an anatomical specialisation key to force mediation [39]. Clinical signs of laminitis (a disease causing lameness) occur when this hierarchical lamella architecture disintegrates [40], thus natural selection pressure should ensure a robust interface [38, 41]. While the extensive surface area available for adhesion is used as justification for the ability of the equine hoof capsule to survive large load [38, 39, 41], no studies have attempted to model this hypothesis. Given the widespread use of equids in developing economies [42–44], and well established economic cost of lameness in cattle [45, 46], comprehending laminitis would make great welfare and economic sense. Understanding the mechanical function of this biological interface is a critical step in alleviating diseases associated with its degradation.

In this paper we present a thorough investigation into the effect of hierarchical geometry on interface stiffness and stress distributions. Using analytic methods, confirmed through finite element work, we demonstrate the dependence of scaling relationships defining interface stiffness on the hierarchical order of the geometry. We find stiffer interfaces are linked with increased hierarchy. In higher order structures, we find that more than one scaling regime exist and we present analytic arguments linking the different scaling regimes to specific deformation modes. Furthermore, we establish that hierarchical geometry leads to a reduced magnitude of stress observed in the material linking the two sides of the interface. Based on this observation, we make predictions about the region of the structure that will first exhibit non-elastic deformations and show this can be manipulated through alterations in the geometry of the interface.

II. GEOMETRY AND HIERARCHY

Here we focus on joining two materials of vastly differing stiffness via an intermediate elastic medium. We assume that the system is rectangular and that the upper region of the system is made up of only the stiffer material while the lower extreme is made up of only the softer material. These two materials can only be joined via the intermediate material. As such, the three materials will be referred to as “upper”, “lower” and “intermediate” referring to their position in the composite (see figure 2). The upper material has a stiffness much greater than the other materials in the structure and as such will be modeled as infinitely stiff. The remaining two materials are both linear elastic with Young’s Modulus and Poisson’s ratio given by Y_i, ν_i and Y_l, ν_l for the intermediate and lower materials respectively. For a given system dimen-

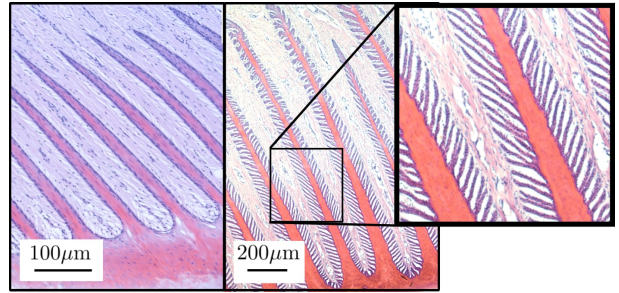


FIG. 1: A cross sectional image taken perpendicular to the surface of the hoof wall. The image shows the interface between soft biological material and stiff keratinized materials found in the bovine (left) and equine (right) hoof. In both cases the hoof wall is situated below the region imaged, while the pedal bone is above. This interface mediates large concussive loads between the two regions during the animal locomotion. The secondary lamellae are on both the dermal and epidermal lamellae are clearly visible in the inset of the right hand image.

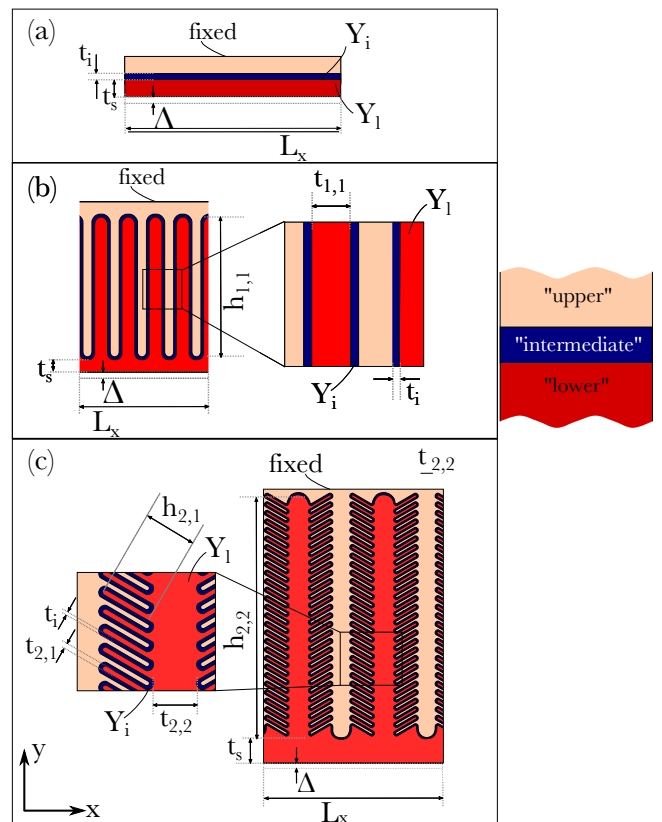


FIG. 2: (a) The generation-0 geometry: a planar connection of two materials of vastly differing stiffness joined by an adhesive connection of thickness t_i . (b) The generation-1 interface and its parameterisation. (c) The generation-2 geometry: A pair of primary lamellae protrude from the deformable domain, from these primary lamellae, a secondary set of lamellae emanate at a given angle, θ ($\theta = \pi/3$ shown). The fixed domain interdigitates these deformable lamellae. In all three diagrams, the cream region represents an infinitely stiff material, which is connected to the deformable material (shown in red) via a (navy-blue) inter-surface interaction. An imposed displacement of Δ is applied to the lower surface of a given design and the stiffness of the interface is evaluated.

sion, a pair of internal boundaries can then be defined specifying the geometry entirely: one boundary defines the transition from the lower to the intermediate material, the second marking the transition from the intermediate to the upper region. The materials at each boundaries are assumed to be perfectly bonded. A possible geometry showing the three material domains is shown in figure 2 (a). In this work, we focus on geometries where the width of the intermediate domain is fixed. We therefore specify a single curve describing the center of the intermediate domain, and we require that the boundaries defining the geometry are a fixed distance $t_i/2$ from this curve; this width is measured in the direction normal to the tangent of the curve at that point.

The geometry investigated here can be described as being of varying “generation”, each generation introduces a new lengthscale into the problem. The generation-0 geometry is shown in figure 2 (a): the boundaries between the different materials form a pair of straight parallel lines. The generation-1 structure is designed such that the two materials to be joined (the upper and lower materials) form a set of interdigitating lamellae whose tips are rounded with semicircular caps. The lamellae introduced are both of equal length $h_{1,1}$ and thickness $t_{1,1}$, this geometry is shown in figure 2 (b). To form the final geometry, we take the generation-1 structure and add a secondary set of interdigitating lamellae along the sides of the primary lamellae, this geometry is shown in figure 2 (c). The angle at which the secondary lamellae protrude from the primary lamellae is set to be θ . We follow the notation used in similar work on hierarchical structures [18, 19, 25]: the parameter X describing the geometry on the i -th lengthscale in a generation G structure is denoted $X_{G,i}$, where $i = G$ is the longest lengthscale, and $i = 1$ is the shortest (thus, for example, $t_{2,1}$ denotes thickness of the secondary lamellae in a generation-2 structure). These geometries along with the notation used in their parameterization is shown in figure 2. An important variable governing the mechanics of these structures is the aspect ratio of the lamellae, we define this as

$$a_{G,i} \equiv \frac{h_{G,i}}{t_{G,i}}. \quad (1)$$

When non-zero forces are applied to the upper and lower boundaries, a relative displacement between the two boundaries will be observed. Due the infinite stiffness of the upper material, the relative displacement of these boundaries signifies deformation in the lower and intermediate materials only. We aim to investigate the effect of geometry, and in particular the addition of substructure, on the stiffness and strength of the interface.

III. RESULTS

Here we present the results of finite element simulations calculating the stiffness of geometries with varying

degrees of hierarchy, alongside analytic scaling results. The finite element simulations are undertaken using the two-dimensional structural mechanics module of COMSOL 5.1 Multiphysics [47] with a plane strain assumption. Mesh refinement studies were undertaken to ascertain accuracy of the results, required mesh density was highly dependent on the relative thickness of interface to lamellae and other parameters (further information on the finite element work performed here can be found in the methods appendix).

A. Stiffness

In order to test the stiffness of the interface, we fix the upper external boundary of the system and investigate the magnitude of force must be applied to the lower external boundary of the system to create a displacement of a given size and direction. The fixed boundaries in the geometries are labeled “fixed” in figure 2, and the displacement considered along the lower external boundary is indicated with a grey dashed line. We only consider small deformations such that the response of the structure is close to linear. Here we investigate structure being loaded under tension as this are the biologically relevant loading condition [48–50]. In order to find the stiffness of a given geometry under tension, we investigate what loading is required to create a deformation of magnitude Δ in the $-y$ direction relative to the upper boundary. Here we report the total loading resulting from the displacement of magnitude Δ and refer to it as a “reaction force” as it arises in response to the imposed displacement.

1. Generation-0

The generation-0 structure is composed of a planar interface between a deformable and an infinitely rigid material connected by an intermediate elastic medium, see figure 2. When imposing a displacement on the base of the deformable surface (the lower external boundary of the system) relative to the infinitely stiff material, the nature of the deformation across the structure will be dependent on the stiffness of the intermediate material, Y_i , and that of the lower material, Y_l , the ratio of the stiffness will be denoted η :

$$\eta = \frac{Y_l}{Y_i}. \quad (2)$$

We also introduce the non-dimensional load parameter,

$$f_R(G) \equiv \frac{F_R(G)}{Y_l \Delta}, \quad (3)$$

where Δ is the imposed displacement on the structure, G denotes the generation of the structure investigated and F_R is the reaction load parallel to the imposed displacement per unit length in the remaining spatial dimension.

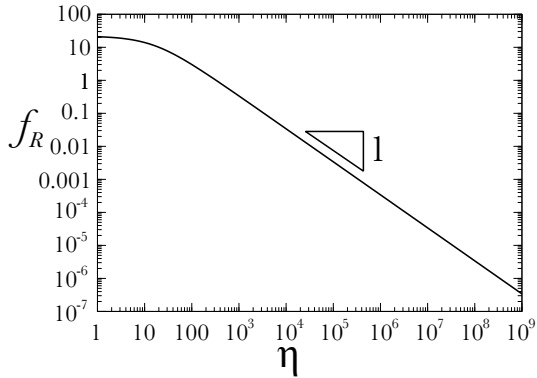


FIG. 3: The stiffness of a generation-0 interface. The reaction force shown is for a structure with parameters $L_x = 3 \times 10^{-4}$ m, $t_i = 1 \times 10^{-6}$ m, $Y_i = 100$ MPa, $\Delta = \frac{t_i}{10}$.

For a fixed geometry and Poisson's ratios, this parameterization collapses all pairs of (Y_i, Y_l) onto a single line. The value of $F_R(0)$ for $\eta \gg 1$ can be calculated noting that in this limit the system closely approximates two rigid bodies exerting a force on the intermediate layer. Thus, the reaction force for a given displacement will be given by,

$$F_R(0) = \frac{Y_i L_x}{t_i} \Delta. \quad (4)$$

From Eq. (3), we thus expect that for sufficiently large η , $f_R \sim \eta^{-1}$; this scaling is shown in figure 3 against results of finite element simulations. This result is used as a benchmark for the more complex hierarchical geometries.

2. Generation-1

For the generation-1 and generation-2 designs, we introduce γ as the ratio of the total reaction force of the structure of interest to that of the generation-0 structure of the same width (L_x in figure 2), undergoing the same deformation,

$$\gamma \equiv \frac{f_R(G)}{f_R(0)}. \quad (5)$$

As shown in figure 2, the generation-1 geometry is made up of a flat interface between a deformable (with Young's Modulus Y_l) and infinitely stiff material with a series of interdigitated lamellae protruding perpendicular to the interface from either side. The two materials are joined by an intermediate material with Young's Modulus Y_i . The parameters used in obtaining the below results are $t_{1,1} = 5 \times 10^{-4}$ m, $t_i = 1 \times 10^{-6}$ m, $t_s = 5 \times 10^{-5}$ m, $Y_i = 1 \times 10^8$ Pa, $\Delta = t_i/10$, and $\nu_l = \nu_i = 0.3$.

We consider tension imposed on the deformable surface: a displacement in the $-y$ direction is imposed along

the lower external boundary of the system, as indicated in figure 2, and the reaction force, F_R on the structure is measured (see appendix A). The maximum value of γ can be approximated through physical considerations. The upper limit of $F_R(1)$ can be calculated noting that for $\eta \gg 1$ ($Y_l \gg Y_i$) the deformation in the structure will be limited to the intermediate material, thus the system will approximate two infinitely stiff bodies joined by the intermediate material of stiffness Y_i (see right hand side colour map in figure 4, the upper and lower material are displaced by uniform amounts). Due to the geometry of the system, the response will be dominated by the region on the intermediate material that experiences shear loading. The force that will be required to induce a displacement of Δ across this material in shear will be

$$F_R(1) = \frac{Y_i a_{1,1} t_{1,1}}{(1 - \nu_i) t_i} \Delta. \quad (6)$$

Thus, in the limit of $\eta \gg 1$, the increase in stiffness compared to a the generation-0 structure (Eq. (4)) will be given by,

$$\gamma = \frac{a_{1,1}}{2(1 - \nu_i)}. \quad (7)$$

This expression is plotted in figure 4 alongside the results of simulations. It is observed in figure 4 that prior to this plateau, γ increases with increasing η , in this regime, the scaling of γ with η can be established through energy considerations: while γ is increasing with increasing η , it is observed that the tips of the lower set of lamellae are displaced less than the lamellae base, the color map on the left in figure 4 shows a typical displacement in this regime. The majority of the deformation within the structure is then limited to a region of the deformable materials close to the lamellae base. Here we introduce the parameter $l_{G,i}^*$, this length describes the distance from the base of the lamellae within which the structure experiences significant deformation, it is defined by an equivalence in energy stored in the deformation of the lamellae structure and an isolated structure of length $l_{G,i}^*$ with suitable boundary conditions experiencing uniform strain (it is noted that l^* is not a quantity related to the geometry of the structure, it is a parameter that varies as a function of η , representing the extent to which the deformations penetrates into the interface structure). The strain energy stored in the lamella structure of the lower material scales in the same way as an isolated beam of width $t_{1,1}$ and length $l_{1,1}^*$ fixed at one end and subject to a displacement Δ extending the structure parallel to its length:

$$U_1 \sim \frac{Y_l t_{1,1}}{l_{1,1}^*} \Delta^2. \quad (8)$$

The strain energy in deforming the intermediate material will scale in the same manner as an elastic material of length $l_{1,1}^*$ subject to a shear displacement of magnitude

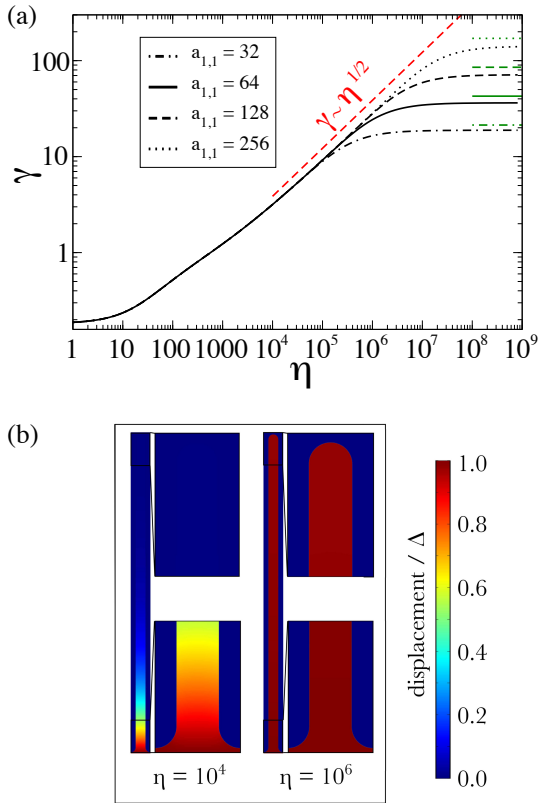


FIG. 4: (a) The stiffness increase of a generation-1 interface relative to a flat geometry (generation-0) as a function of η . The interface loaded under tension and the stiffness of the interface is measured (see appendix A). The figure shows the results for various aspect ratios of structure, $a_{1,1}$, as defined in Eq. (1). The maximum values of γ as predicted in Eq. (7) are shown in green lines, the results of simulations get closer to these predicted values in the limit of large η . The scaling of $\gamma \sim \eta^{1/2}$ is shown in red, this scaling was predicted in Eq. (10). (b) Colour maps indicating the magnitude of the displacement of the lamella ($a_{1,1} = 32$); for $\eta = 10^4$ close to zero displacement is observed at the tip of the lamella structure while for $\eta = 10^6$, the whole lamella approximates a rigid body and thus the value of γ plateaus. For both left and right, the parameters used are described in the main text.

Δ :

$$U_i \sim \frac{Y_i l_{1,1}^*}{(1 - \nu_i) t_i} \Delta^2. \quad (9)$$

Selecting the value of $l_{1,1}^*$ that minimizes the internal energy ($U_i + U_1$) in the system, assuming non-zero displacement Δ , we find the scaling $l_{1,1}^* \sim \eta^{1/2}$. Using Eq. (4, 5 and 7), for fixed $t_{1,1}$, we see that in this regime,

$$\gamma \sim \eta^{1/2}. \quad (10)$$

This scaling is plotted in figure 4 alongside the results of finite element simulations.

Fitting the results of finite element work within an appropriate range of η gives a scaling of $\gamma \sim \eta^{0.50}$, where the error in the power is ± 0.01 .

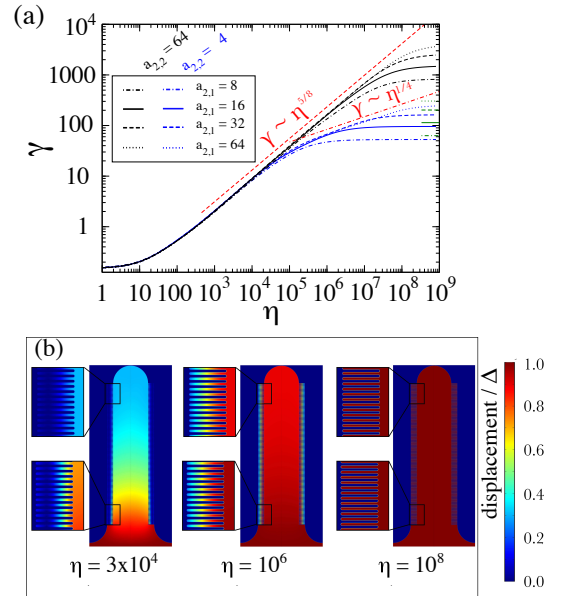


FIG. 5: (a) The stiffness increase of a generation-2 interface relative to a generation-0 geometry for various values of aspect ratio. The interface loaded under tension and the stiffness of the interface is measured. The results are shown for various structures where the aspect ratio of both the primary and secondary lamellae ($a_{2,2}$ and $a_{2,1}$ respectively) have been varied. (b) Snapshots of simulations showing the displacement on the lamella structure for various η with $a_{2,2} = 4$, $a_{2,1} = 16$: $\eta = 3 \times 10^3$ is in the regime whereby increasing η serves to increase displacement towards the tips of the primary and secondary lamellae; at $\eta = 10^6$ the primary lamella acts close to a rigid body (the displacement at the tip of the lamella is over 90% of that at the base), increasing η serves primarily to increase the displacement towards the tip of the secondary lamellae; for $\eta = 10^8$ all lamellae structures move as rigid bodies, almost all strain is observed in the intermediate material. These three snapshots are from the regimes of $\gamma \sim \eta^{5/8}$, $\gamma \sim \eta^{1/4}$ and γ independent of η respectively.

3. Generation-2

Here, we establish the mechanical response of the generation-2 structure when the lower external boundary is displaced under tension. In this structure, the lower material makes up two sets of lamellae: the primary lamellae of length and thickness $h_{2,2}$ and $t_{2,2}$ and the secondary lamellae described by the parameters $h_{2,1}$ and $t_{2,1}$. We perform finite element simulations on structures whose primary and secondary lamellae have a range of aspect ratios between 4 and 64; the effect of other parameters can be elucidated from the analytic work presented below. The parameters used in the simulations presented here are $h_{2,1} = 8 \times 10^{-5}$ m, $t_{2,2} = 5 \times 10^{-4}$ m, $t_i = 10^{-6}$ m, $t_s = 5 \times 10^{-5}$ m, $Y_i = 10^8$ Pa, $\Delta = t_i/10$ and $\nu_i = \nu_i = 0.3$, other geometric and material parameters are given by a specific aspect ratio and η value.

We analyze the response of the structure when a displacement in the $-y$ direction is imposed on lower external boundary, as indicated in figure 2. In the limit

of large η ($Y_i \ll Y_l$), any imposed displacement on the external boundary of the lower material will indicate a deformation in the intermediate material, a typical deformation in this regime is shown in the right hand side color map in figure 5 where the lower material shows a uniform displacement. The force required to impose a given displacement in this limit can be approximated as:

$$F_2 = \frac{4h_{2,2}h_{2,1}Y_i}{2t_it_{2,1}}. \quad (11)$$

Using Eq. (4), the maximum value for γ can then be calculated, this maximum value is indicated in figure 5 for $a_{2,2} = 4$. For small $a_{2,2}$ and large $a_{2,1}$, we observe a scaling law immediately before γ reaches its plateau. We hypothesize that this scaling law is observed when the primary lamellae in the structure closely resemble rigid bodies, and the secondary lamellae experience a deformation within a distance $l_{2,1}^*$ of their connection with the primary lamellae, a snapshot from a simulation showing typical deformation in this regime is shown in figure 5 (middle). We support this hypothesis with a scaling argument: in this regime the secondary lamellae will bend, the energy associated with this slender structure of length $l_{2,1}^*$ and thickness $t_{2,1}$, bending with a displacement Δ at its tip scales as:

$$U_1 \sim \frac{Y_l t_{2,1}^3}{l_{2,1}^3} \Delta^2. \quad (12)$$

The strain energy in the interface will scale as a tension/compression strain of magnitude Δ/t_i imposed over a region $l_{2,1}^*$ in length, thus

$$U_i \sim \frac{Y_i l_{2,1}^*}{t_i} \Delta^2. \quad (13)$$

Selecting the value of $l_{2,1}^*$ so as to minimize the internal energy of deformation (assuming non-zero Δ), we find that $l_{2,1}^* \sim \eta^{1/4}$. Given the force the structure will support will be proportional to the area over which strain is spread (Eq. (11)), we see that in this regime

$$\gamma \sim \eta^{1/4}. \quad (14)$$

For sufficiently large values of $a_{2,2}$ and $a_{2,1}$ prior to the $\gamma \sim \eta^{1/4}$ regime we observe a second scaling law. In this regime both the primary and secondary lamellae will deform within a characteristic length $l_{2,2}^*$ and $l_{2,1}^*$ respectively (where $l_{2,2}^* < h_{2,2}$ and $l_{2,1}^* < h_{2,1}$). Here, increasing η will serve to increase $l_{2,1}^*$ and $l_{2,2}^*$. The scaling of $l_{2,2}^*$ can be calculated by considering the energy of deformation of both the lower material and the intermediate material, these are given by

$$U_s \sim Y_s \left(\frac{t_{2,2}}{l_{2,2}^*} + \frac{t_{2,1} l_{2,2}^*}{l_{2,1}^* t_{2,1}} \right) \Delta^2, \quad U_i \sim \frac{Y_i l_{2,1}^* l_{2,2}^*}{t_i t_{2,1}} \Delta^2. \quad (15)$$

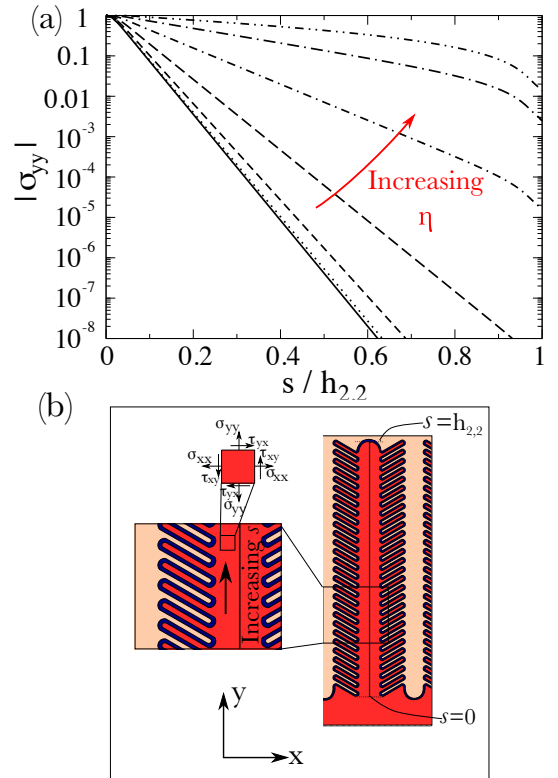


FIG. 6: (a) Semi-log plot of σ_{yy} down the centre of the primary lamella as a function of distance from the lamella base for a particular structure ($a_{2,2} = 16, a_{2,1} = 4$ with all other dimensions as given in previous section), for values of $\eta = 10^n$ with integer n from 0 to 7. An exponential decay in the magnitude of the stress for values of η smaller than that taken for γ to plateau (see figure 5) is observed. (b) A schematic showing the region in which σ_{yy} is evaluated.

The expression for U_l is made up of two terms, the stretching of the primary lamellae (first term) and the bending of the secondary lamellae (second term). Selecting the value of $l_{2,2}^*$ that minimizes the total energy of the system (for a non-zero displacement Δ), noting that $l_{2,1}^* \sim \eta^{1/4}$, we see that for $\eta \gg 1$, $l_{2,2}^* \sim \eta^{3/8}$. Thus from Eqs. (4, 5 and 11), we see that in this regime,

$$\gamma \sim \eta^{5/8}. \quad (16)$$

These scaling laws are shown in figure 5 alongside the results of finite element simulations.

B. Stress distribution and hierarchy

In this section we investigate the stress distributions present within the hierarchical lamellae structures to further elucidate the mechanics of the system. First, we establish the nature of the stresses within the primary lamellae as a function of distance from the lamellae base. We then show the dependence of the maximal von Mises stress within the structure on the interface geometry. Fi-

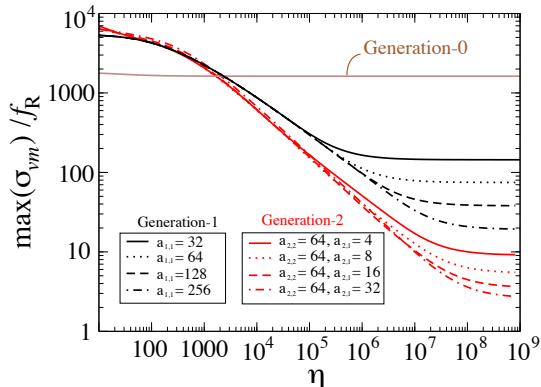


FIG. 7: The maximal von Mises stress observed in the interface material, scaled by the total reaction force on the boundary of a set of generation-0, 1 and 2 structures. For values of η greater than 10^3 , it is observed that hierarchical structures better protect the interface material from high magnitude stresses and generation-2 structures out perform the generation-1 geometries.

nally, we make a hypothesis on the region in which failure is likely to initiate for various geometries.

We first examine the magnitude of the σ_{yy} component of stress down the center of the primary lamellae in the generation-1 and 2 structures. We find that for both the generation-1 and 2 structures, the magnitude of the stress decreases with an exponential decay as a function of distance from the lamella base, s , that is, $|\sigma_{yy}| \sim \exp(-ks)$, see figure 6. For a given geometry, the value of k varies as a function of η , the relative stiffness of the intermediate and lower materials. For sufficiently large η the decay is no longer exponential, this coincides with γ reaching its plateau value.

In figure 7, we present the maximum value of the von Mises stress ($\sigma_{vm} = \sqrt{\sigma_{xx}^2 + \sigma_{yy}^2 - \sigma_{xx}\sigma_{yy} + 3\tau_{xy}^2}$) present within the intermediate material, scaled by the reaction force at the boundary where the displacement is imposed. This measure gives an indication of how effective the geometry is at creating a strong adhesive connection utilizing a weak connective material. It is found that for values of η greater than approximately 10^3 , hierarchical geometries provide an advantage in terms of loading withstood for a given intermediate material stress. The generation-2 structure investigated here provides advantages over the generation-1 for values of η larger than approximately 10^3 .

Finally we look at the expected failure region of the structure, and the effect of hierarchy. The structure considered here is made of two deformable materials, the intermediate material and the lower material (navy and red in figure 2). These two materials can be assigned a yield stress, σ_{Y1} and σ_{Y2} for the intermediate and the lower materials respectively. When the structure is loaded, either material can initiate plastic deformation, this will occur when the maximum von Mises stress exceeds the yield stress of the material. For a given ge-

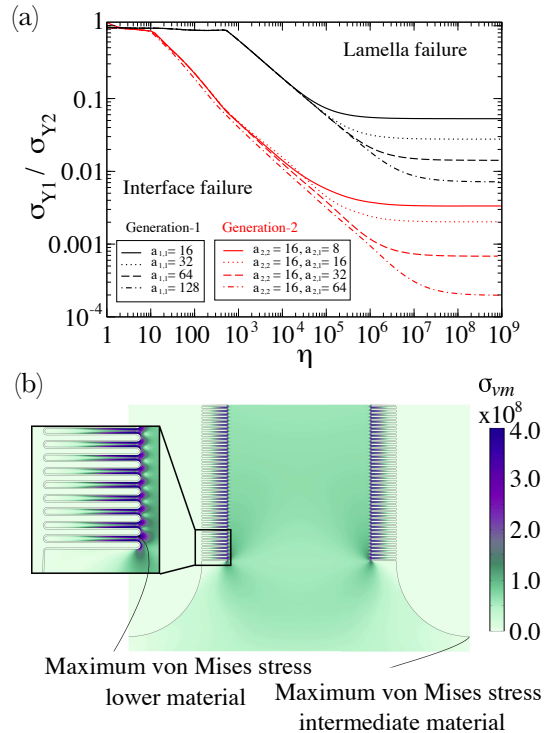


FIG. 8: (a) The expected region of failure in the structure connecting two different materials. Above the curve describing a given geometry, the material making up the lamella structure will experience non-elastic deformation before the interface material, and the reverse occurs below. (b) The location of the maximum stresses in a particular generation-2 structure where the colour-map indicates the magnitude of the von Mises stress at that point.

ometry, the region in which non-elastic deformation first occurs depends on the value of η considered and the ratio of σ_{Y1}/σ_{Y2} . To establish the region that will exhibit non-elastic deformation first, we use the following procedure: impose a displacement on the lower external boundary of the structure in the $-y$ direction (as in the investigations into stiffness); then establish the maximum von Mises stress in the two deformable domains; assuming non-elastic deformations occur before large geometric non-linearities are observed, the ratio of these maximum stresses indicate the ratio of σ_{Y1} to σ_{Y2} for which the region of failure transitions from the interface to the lamellae. The space $(\eta, \sigma_{Y1}/\sigma_{Y2})$ can then be split into the two regions shown in figure 8. For low values of η and a low ratio σ_{Y1}/σ_{Y2} , we see the intermediate material will fail first for both generation-1 and -2 structures, while for sufficiently high values of η and high ratios σ_{Y1}/σ_{Y2} , plastic deformation in the lower material will occur first.

IV. SUMMARY

We have shown that a geometry based on that observed in the equine hoof is conducive to a stiff interface between two materials of vastly differing stiffness. We

have demonstrated that through increasing the number of length-scales within the structure, the scaling laws relating stiffness of the constituent materials to the global interface stiffness can be manipulated in a systematic manner. We have linked these different scaling regimes with different deformation modes within the structure and supported these hypotheses with scaling law arguments. Furthermore, we have found through altering the aspect ratio of the lamellae, the value of η at the transition from one scaling regime to another can be manipulated.

We have shown that the hierarchical geometry leads to a reduced maximal stress observed in the intermediate material for a given magnitude of loading. Furthermore, we have demonstrated that the ratio of maximal stresses in the intermediate material to those in the lamellae can be manipulated over orders of magnitude through alterations in the geometry of the structure. These findings are of particular relevance given the recent growth of digital manufacturing techniques which allow for the fabrication of 2-d structures with features on nano/micro length-scale [51]. In many areas of application, the materials to be joined may be specified by the functionality of the desired structure, thus the parameter η is set by the application. For a given η , we have shown that through close control of geometry, it is possible to create interfaces with high stiffness, a selectable failure mode, and tailorable stresses within the interface material. This methodology thus allows for enhanced functionality of structures through permitting a less restricted choice of constituent materials.

In principle higher generation structures could be created by adding further substructure to the generation-2 geometry proposed here. It is hypothesised that the addition of extra substructures would further alter the scaling relationships established here, and it is thought that such a structure would exhibit similar trends to those observed in other hierarchical metamaterials whereby the scaling tends towards a well defined limit [25]. Though this work shows the tailorability of interface stiffness through hierarchy, open questions remain regarding the fracture properties, ductility and strength of these intricate architectures.

This work highlights the general importance of geometry in the creation of joints between dissimilar materials, allowing for composite and hybrid structures with enhanced structural efficiency [32]. A natural application for this composite joint is to be found in medical implants where high performance joints between dissimilar materials is of key importance. Here, the tailorability of the resultant joint and the use of an intermediate material that experiences minimal mechanical stresses is of great practical importance as it permits the reduction of stress concentrations and greater biocompatibility [32]. Our work also offers a new perspective on the development of tendon-bone interfaces where the low success rates of graft implantation alongside the increased occurrence of musculoskeletal injuries necessitate the development of

novel repair strategies [53]. Furthermore, it is widely observed that natural composites simultaneously exhibit high stiffness and fracture resistance [13, 14], it is hypothesized here that through designing the interface between the different constituent materials, one can achieve meta-materials that match or exceed their naturally occurring analogues.

Not only does this work have implications for the design of geometry in the engineering challenge of joining two materials of differing stiffness, this work also lends credence to the long assumed role of hierarchical interface geometry in the equine hoof: such geometry has been selected by evolutionary pressures (among other reasons) for mechanical purpose. Despite the undoubted complexity of the biological system, it is expected that the main findings of this work apply to the interface observed within the hoof: increasing the hierarchy of the interface serves to increase the mechanical stiffness of the interface (this is also notable for the previously reported link between stiffness and strength of composite structures, it is widely observed that the presence of one implies the other [52]). We believe that with more theoretical analysis of hierarchical structures, together with increased ability to fabricate these intricate architectures, hierarchical architectures will become more widely utilised in engineering designs of the future.

V. ACKNOWLEDGMENTS

The authors would like to thank Catrin Rutland, David Neal, and Ramzi Al-Agele. D.R.-K. would like to acknowledge funding support from the Academy of Finland. D.R.-K. would like to thank Giulio Costantini for useful discussions regarding this manuscript. C.R. acknowledges funding support from Petplan charitable trust and Waltham.

Appendix A: Methods

All simulations presented in this work have been undertaken using solid mechanics module of COMSOL 5.1 performing ‘stationary’ (quasi-static) studies. The geometry is made up of three materials, as shown in figure 2, the upper material is modeled as infinitely stiff (using the inbuilt ‘rigid domain’ option of COMSOL). The remaining two materials are linear elastic and described by the parameters given in the main text. Meshing was performed using the inbuilt COMSOL routines, mesh refinement studies to be performed establishing the accuracy of the results (checking for convergence of results). The upper external boundary was then fixed in space, while the lower external boundary had a displacement imposed on it in the $-y$ direction, as shown in figure 2. The equilibrium position of the structure was then obtained and the reaction force on the lower boundary was evaluated through integration (inbuilt COMSOL routine). This re-

action force is equivalent to the force that would be required to induce the considered displacement.

-
- [1] W. Federle, Why are so many adhesive pads hairy? *J. Exp. Biol.* **209**, 2611 (2006).
- [2] H. Yao and H. Gao, Mechanics of robust and releasable adhesion in biology: Bottomup designed hierarchical structures of gecko. *J. Mech. Phys. Solids* **54**, 1120 (2006).
- [3] D. Labonte, C. J. Clemente, A. Dittrich, C.-Y. Kuo, A. J. Crosby, D. J. Irschick, and W. Federle., Extreme positive allometry of animal adhesive pads and the size limits of adhesion-based climbing. *Proc. Natl Acad. Sci.* **113**, 1297 (2016)
- [4] G. Huber, H. Mantz, R. Spolenak, K. Mecke, K. Jacobs, S. N. Gorb, and E. Arzt, Evidence for capillarity contributions to gecko adhesion from single spatula nanomechanical measurements. *Proc. Natl Acad. Sci.* **102**, 293 (2005).
- [5] W. J. Stewart, and T. E. Higham, Passively stuck: death does not affect gecko adhesion strength. *Bio. Lett.* **10**, 20140701 (2014)
- [6] K. Autumn, M. Sitti, Y. A. Liang, A. M. Peattie, W. R. Hansen, S. Sponberg, T. W. Kenny, R. Fearing, J. N. Israelachvili, and R. J. Full, Evidence for van der Waals adhesion in gecko setae. *Proc. Natl Acad. Sci.* **99**, 12252 (2002)
- [7] H. Yao and H. Gao (2013) *Mechanics of Self-Similar Hierarchical Adhesive Structures Inspired by Gecko Feet*. In: *Structural Interfaces and Attachments in Biology*. (eds. Thomopoulos S., Birman V., Genin G.) Springer, New York, NY
- [8] M. R. Cutkosky, Climbing with adhesion: from bioinspiration to biounderstanding. *Interface Focus* **5**, 20150015 (2015)
- [9] A. K. Geim, S. V. Dubonos, I. V. Grigorieva, K. S. Novoselov, A. A. Zhukov and S. Yu. Shapoval, Microfabricated adhesive mimicking gecko foot-hair *Nat. Mat.* **2**, 461 (2003)
- [10] D. Brodoceanu, C. T. Bauer, E. Kroner, E. Arzt, T. Kraus, Hierarchical bioinspired adhesive surfaces a review. *Bioinspir. Biomim.* **11**, 051001 (2016)
- [11] K. Autumn and N. Gravish, Gecko adhesion: evolutionary nanotechnology. *Phil. Trans. R. Soc. A* **366**, 1575 (2008)
- [12] H. Zhou and Y. Zhang, Hierarchical chain model of spider capture silk elasticity. *Phys. Rev. Lett.* **94**, 028104 (2005)
- [13] R. O. Ritchie, The conflicts between strength and toughness. *Nat. Mater.* **10**, 817822 (2011)
- [14] Y. Li, C. Ortiz and M. C. Boyce, Bioinspired, mechanical, deterministic fractal model for hierarchical suture joints. *Phys. Rev. E* **85**, 031901 (2012).
- [15] R. Huiskes, R. Ruimerman, G. H. van Lenthe and J. D. Janssen, Effects of mechanical forces on maintenance and adaptation of form in trabecular bone. *Nature* **405**, 704 (2000)
- [16] T. A. Schaefer, A. J. Jacobsen, A. Torrents, A. E. Sorensen, J. Lian, J. R. Greer, L. Valdevit, and W. B. Carter, Ultralight metallic microlattices. *Science* **334**, 962 (2011)
- [17] E. Lin, Y. Li, J. C. Weaver, C. Ortiz and M. C. Boyce, Tunability and enhancement of mechanical behavior with additively manufactured bio-inspired hierarchical suture interfaces. *J. Mat. Res.* **9**, 1867 (2014)
- [18] D. Rayneau-Kirkhope, Y. Mao, and R. S. Farr, Optimization of fractal space frames under gentle compressive load. *Phys. Rev. E* **87**, 063204 (2013)
- [19] D. Rayneau-Kirkhope, Y. Mao and R. S. Farr, Ultralight Fractal Structures from Hollow Tubes. *Phys. Rev. Lett.* **109** 204301 (2012)
- [20] P. Reis, H. Jaeger and M. van Hecke, Designer Matter: A perspective. *Ext. Mech. Lett.*, **5** 25 (2015)
- [21] T. Mullin, W. Deschanel, K. Bertoldi and M. C. Boyce, Pattern Transformation Triggered by Deformation. *Phys. Rev. Lett* **99**, 084301 (2007)
- [22] K. Bertoldi, P. M. Reis, S. Willshaw, and T. Mullin, Negative Poissons Ratio Behavior Induced by an Elastic Instability. *Advanced Materials*, **22**, 361 (2010)
- [23] B. Florijn, C. Coulais, and M. van Hecke, Programmable Mechanical Metamaterials. *Phys. Rev. Lett.* **113** 175503 (2014)
- [24] T. Buckmann, M. Kadic, R. Schittny, and M. Wegener, Mechanical cloak design by direct lattice transformation. *Proc. Nat. Academy Sci.*, **112** 4930 (2015)
- [25] D. Rayneau-Kirkhope, Y. Mao, and R. S. Farr, Ultralight hierarchical meta-materials on a body-centred cubic lattice. *EPL* **119**, 14001 (2017)
- [26] E. Lin, Y. Li, C. Ortiz and M. C. Boyce, 3D printed, bio-inspired prototypes and analytical models for structured suture interfaces with geometrically-tuned deformation and failure behavior. *J. Mech. Phys. Solids* **73**, 166 (2014)
- [27] Y. Li, C. Ortiz, and M. C. Boyce, Stiffness and strength of suture joints in nature. *Phys. Rev. E* **84**, 062904 (2012)
- [28] Y. Li, C. Ortiz, and M. C. Boyce, A generalized mechanical model for suture interfaces of arbitrary geometry. *J. Mech. Phys. Solids* **61**, 1144-1167 (2013)
- [29] S. Krauss, E. Monsonogo-Ornan, E. Zelzer, P. Fratzl, and R. Shahar, Mechanical Function of a Complex Three-Dimensional Suture Joining the Bony Elements in the Shell of the Red-Eared Slider Turtle. *Adv. Mat.* **21** 407 (2009)
- [30] R. P. Hubbard, J. W. Melvin and I. T. Barodawala, Flexure of cranial sutures. *J. Biomechanics* **4**, 491 (1971)
- [31] S. Inoue, and S. Kondo, Suture pattern formation in ammonites and the unknown rear mantle structure. *Sci. Rep.*, **6**, 33689 (2016)
- [32] R. W. Messler, Jr, *Joining of Materials and Structures: From pragmatic process to enabling technology* Elsevier Butterworth-Heinemann, Burlington USA (2004)
- [33] J. E. Stump, Anatomy of the normal equine foot, including microscopic features of the laminar region. *J. Am. Vet. Med. Assoc.* **151** 1588-1598 (1967)
- [34] R. A. Kainer, Clinical Anatomy of the Equine Foot., *Vet. Clin. North Am. Equine Pract.* **5** -271 (1989)
- [35] C. C. Pollitt, The anatomy and physiology of the hoof wall. *Equine Vet Educ* **10**, 318-325 (1998)
- [36] M. G. Farquhar and G. E. Palade, Junctional Complexes in Various Epithelia. *Journal of Cell Biology*, **17** 375 (1963)

- [37] C. Rauch and M. Cherkaoui-Rbati, Physics of nail conditions: why do ingrown nails always happen in the big toes? *Physical biology*, **11**, 066004 (2014)
- [38] C. C. Pollitt, Anatomy and physiology of the inner hoof wall. *Clinical Techniques in Equine Practice* **3** 3-21 (2004)
- [39] C. C. Pollitt, The anatomy and physiology of the hoof wall. *Equine Vet. Educ.* **10**, 318-325 (1996)
- [40] C. C. Pollitt, Equine laminitis: A revised pathophysiology. *AAEP Proc.* **45**, 188 (1999)
- [41] C. C. Pollitt, Laminitic Pain: Parallels with Pain States in Humans and Other Species. *The Veterinary clinics of North America Equine practice* **26**, 643 (2010)
- [42] J. C. Pritchard, A. C. Lindberg, D. C. Main and H. R. Why, Assessment of the welfare of working horses, mules and donkeys, using health and behaviour parameters. *Prev Vet Med.* Jul 12;69(3-4):265-83 (2005)
- [43] A. Doumbia, The Contribution of working donkeys to the livelihoods of the population in Mali, *Society for the Protection of Animals Abroad, Presented at the 7th International Colloquium on Working Equids, London, UK*, (2014)
- [44] J. Pritchard, M. Upjohn and T. Hirson, Improving working equine welfare in 'hard-win' situations, where gains are difficult, expensive or marginal. *PLoS One.* Feb 6;13(2):e0191950 (2018)
- [45] J. J. Vermunt, "Subclinical" laminitis in dairy cattle. *N Z Vet J.* 40 133-8 (1992)
- [46] C. Lischer and P. Ossent, Laminitis in cattle: a literature review, *Tierarztl. Prax.* **22** 424-32 (1994).
- [47] COMSOL Inc., <http://www.comsol.com/comsol-multiphysics>
- [48] J. E. Douglas and J. J. Thomason, Shape, orientation and spacing of the primary epidermal laminae in the hooves of neonatal and adult horses (*Equus caballus*). *Cells Tissues Organs* **166** 304 (2000)
- [49] B. Faramarzi, Morphological spectrum of primary epidermal laminae in the forehoof of Thoroughbred horses. *Equine Vet. J.*, **43** 732 (2011)
- [50] J. J. Thomason, J. E. Douglas and W. Sears, Morphology of the laminar junction in relation to the shape of the hoof capsule and distal phalanx in adult horses (*Equus caballus*). *Cells Tissues Organs*, **168** 295 (2001)
- [51] J. Valente, E. Plum, I. Youngs and N. Zheludev, Nano- and Micro-Auxetic Plasmonic Materials. *Adv. Mat.* **28** 5176 (2016)
- [52] F. Barthelat and M. Mirkhalaf, The quest for stiff, strong and tough hybrid materials: an exhaustive exploration. *J. R. Soc. Interface* **10** 20130711 (2013)
- [53] J. Z. Paxton, K. Baar, L. M. Grover, Current Progress in Enthesis Repair: Strategies for Interfacial Tissue Engineering, *Orthopedic & Muscular System* S1:003 2161-0533 (2012)